

The role of dust in “active” and “passive” low-metallicity star formation

H. Hirashita^{1,*} and L. K. Hunt²

¹ Graduate School of Science, Nagoya University, Furo-cho, Chikusa-ku, Nagoya, 464-8602, Japan
e-mail: hirashita@u.phys.nagoya-u.ac.jp

² Istituto di Radioastronomia-Sezione Firenze, Largo E. Fermi, 5, 50125 Firenze, Italy
e-mail: hunt@arcetri.astro.it

Received 10 December 2003 / Accepted 1 April 2004

Abstract. We investigate the role of dust in star formation activity of extremely metal-poor blue compact dwarf galaxies (BCDs). Observations suggest that star formation in BCDs occurs in two different regimes: “active” and “passive”. The “active” BCDs host super star clusters (SSCs), and are characterised by compact size, rich H₂ content, large dust optical depth, and high dust temperature; the “passive” BCDs are more diffuse with cooler dust, and lack SSCs and large amounts of H₂. By treating physical processes concerning formation of stars and dust, we are able to simultaneously reproduce all the above properties of both modes of star formation (active and passive). We find that the difference between the two regimes can be understood through the variation of the “compactness” of the star-forming region: an “active” mode emerges if the region is compact (with radius $\lesssim 50$ pc) and dense (with gas number density $\gtrsim 500$ cm⁻³). The dust, supplied from Type II supernovae in a compact star-forming region, effectively reprocesses the heating photons into the infrared and induces a rapid H₂ formation over a period of several Myr. This explains the high infrared luminosity, high dust temperature, and large H₂ content of active BCDs. Moreover, the gas in “active” galaxies cools ($\lesssim 300$ K) on a few dynamical timescales, producing a “run-away” star formation episode because of the favourable (cool) conditions. The mild extinction and relatively low molecular content of passive BCDs can also be explained by the same model if we assume a diffuse region (with radius $\gtrsim 100$ pc and gas number density $\lesssim 100$ cm⁻³). We finally discuss primordial star formation in high-redshift galaxies in the context of the “active” and “passive” star formation scenario.

Key words. ISM: dust, extinction — galaxies: dwarf — galaxies: evolution — galaxies: ISM — stars: formation

1. Introduction

The surfaces of interstellar dust grains are known to be sites where efficient formation of hydrogen molecules (H₂) takes place. Without dust grains, H₂ forms only in the gas phase with a production rate much lower than the dust surface reaction (e.g., Peebles & Dicke 1968; Matsuda et al. 1969). The shielding of H₂ dissociating photons by dust grains also enhances molecule formation. In general, dust also absorbs a part of the radiation from stars and reemits it in the infrared (IR)¹, thereby modifying the spectral energy distribution (SED) of galaxies (e.g., Silva et al. 1998). Therefore, dust plays an important role in both chemical and radiative properties of galaxies.

Send offprint requests to: H. Hirashita,
e-mail: hirashita@u.phys.nagoya-u.ac.jp

* Research Fellow of the Japan Society for the Promotion of Science.

¹ In this paper, IR indicates the wavelength range where the emission from dust dominates the radiative energy (roughly 8–1000 μ m).

Recently Hirashita & Ferrara (2002, hereafter HF02) have proposed that the dust enrichment in extremely metal-poor primeval objects is essential for the enhancement of star formation activity. Their scenario suggests the following cycle between dust production and star formation: (i) massive stars end their lives as Type II supernovae (SNe II), which supply dust grains into the interstellar medium (ISM) (Kozasa et al. 1989; Todini & Ferrara 2001; Nozawa et al. 2003; Schneider et al. 2004); (ii) those grains enhance the formation of molecular clouds in which stars form; (iii) some of those stars are massive and the dust supply described in (i) occurs again. This cycle (i)–(iii) effectively enhances the star formation rate as shown by HF02.

In fact, a large amount of dust has been suggested to exist at high redshift (high z) (e.g., Smail et al. 1997). However, it is not easy to explore the first dust enrichment in primeval galaxies at high z ($z \gtrsim 5$) with the present observational facilities. Therefore, nearby templates for primeval galaxies are useful to test galaxy for-

mation scenarios. The best candidates for such a template are metal-poor blue compact dwarf galaxies (BCDs), since they are at the initial stage of metal enrichment and their current star formation activity is generally young (Searle & Sargent 1972; Kunth & Östlin 2000). In other words, BCDs can be used as laboratories in which to study high- z primeval galaxies.

Two classes of star formation activity have recently emerged observationally, as proposed for a BCD sample by Hunt et al. (2003a, hereafter HHTIV; 2004b). They argue that the star-formation activity in the two most metal-poor galaxies, SBS 0335–052 and I Zw 18, shows very different properties, in spite of their similar metallicities ($1/41$ and $1/50 Z_{\odot}$, respectively; Skillman & Kennicutt 1993; Izotov et al. 1999). The major star-forming region of SBS 0335–052 is compact and dense (radius $r_{\text{SF}} \lesssim 40$ pc, number density $n \gtrsim 600 \text{ cm}^{-3}$; Dale et al. 2001; Izotov & Thuan 1999). Moreover, SBS 0335–052 hosts several super star clusters (SSCs), detectable H_2 emission lines in the near-infrared (Vanzi et al. 2000), a large dust extinction ($A_V \sim 16$ mag; Thuan et al. 1999; Hunt et al. 2001; Plante & Sauvage 2002), and high dust temperature (Hunt et al. 2001; Dale et al. 2001; Takeuchi et al. 2003). On the contrary, the star-forming regions in I Zw 18 are diffuse ($r_{\text{SF}} \gtrsim 100$ pc, $n \lesssim 100 \text{ cm}^{-3}$), and contain no SSCs. Near-infrared H_2 emission has not been detected (Hunt et al., private communication), and the dust extinction is moderate ($A_V \sim 0.2$ mag; Cannon et al. 2002). We call a region with such properties “passive” following HHTIV. The similar metallicities of SBS 0335–052 (active) and I Zw 18 (passive) imply that the chemical abundance is not a primary factor in determining the star-forming properties. We argue that the compactness of star-forming regions, which affect gas density, gas dynamics, and so on, is important in the dichotomy of active and passive modes.

Hirashita et al. 2002 (hereafter HHF02) show that the IR luminosity, the dust mass, and the rich H_2 content of SBS 0335–052 can be explained through dust accumulation by successive SNe II in a compact ($r_{\text{SF}} \lesssim 100$ pc) region. Moreover, SBS 0335–052 is not unique among BCDs; the BCDs with dense compact star-forming regions similar to SBS 0335–052 were dubbed “active”, and tend to be characterized by high surface brightness (see Figure 1 of HHTIV). The physical state of ISM is also similar among “active” BCDs. They always have large dust extinction, and a significant fraction of stellar radiation is reprocessed into IR; the dust temperature is also high and there is a “hot” component with 600–1000 K (Hunt et al. 2002). Dust properties can be further constrained by future IR observations for a large sample of BCDs (e.g., Takeuchi et al. 2003). HHTIV also demonstrate that there are BCDs with converse properties, namely “passive” ones, which are more diffuse, less dense, and of lower surface brightness. A representative of this category is I Zw 18. Contrary to “active” BCDs, IR dust emission has not been detected so far in “passive” BCDs. Although their star formation rate is lower than “active” BCDs, “passive” BCDs are actually forming stars, and are com-

pletely different from passively evolving galaxies such as ellipticals.

The above clear difference in dust properties implies that in addition to the compactness, dust should be considered as a key to understand the “active” and “passive” modes, and hence to understanding how star formation occurs in extremely low-metallicity environments. We consider the role of dust in various compactness of regions by using our theoretical framework. This paper is organised as follows. First, in Section 2 we explain the model that describes the evolution of dust content and gas state in a star-forming region. Then, in Section 3, we present our results concerning the differences between “active” and “passive” star-forming regions. In Section 4, we discuss the interpretation of observational properties of active and passive BCDs in the context of our model, and consider in particular the two prototypes, I Zw 18 and SBS 0335–052. Implications for high-redshift star formation are described in Section 5, and our conclusions are presented in Section 6.

2. Model description

For our calculation of dust amount in a star-forming region, we essentially use the model by HF02. We treat the chemical reaction network concerning H_2 formation in a way consistent with dust amount evolution. We approximate star-forming regions as homogeneous spheres and adopt a representative value for each physical quantity (i.e., we treat a star-forming region as one zone).

2.1. ISM evolution

The star formation process is affected by the physical state of the ISM. In metal-poor environments, cooling by molecular hydrogen plays an important role in star formation (Galli & Palla 1998; Abel et al. 2000; Bromm et al. 2001; Nishi et al. 1998; Omukai 2000; Kamaya & Silk 2002; Ripamonti et al. 2002). The abundance of H_2 should be ultimately a key parameter since stars are only seen to form in molecular complexes (see e.g., Wilson et al. 2000 for a recent observation of a nearby galaxy). Moreover, enhancement of molecular gas formation is shown to result in an active star formation (for recent results, see e.g., Walter et al. 2002), and indeed there is a correlation between molecular amount and star formation rate (e.g., Bendo et al. 2002). We define the molecular fraction, f_{H_2} , as

$$f_{\text{H}_2} \equiv 2n_{\text{H}_2}/n_{\text{H}}, \quad (1)$$

where n_{H} and n_{H_2} are the number densities of hydrogen nuclei and hydrogen molecules, respectively (i.e., if all the hydrogen nuclei are in the molecular form, $f_{\text{H}_2} = 1$).

We then calculate the time evolution of ionisation degree (x), molecular fraction (f_{H_2}), and gas temperature (T) of the hydrogen gas. The helium content is neglected here, since its effect should be negligible for the three quantities (Kitayama et al. 2001; HF02). Therefore, the

number density of the gas (n) is approximated by the hydrogen number density (i.e., $n \simeq n_{\text{H}}$). The ionisation degree and the temperature affect the formation rate of H_2 . The processes are treated as follows (see HF02 for details).

We calculate the time evolution of the ionisation degree x by taking into account collisional ionisation, recombination, and photo-ionisation of hydrogen. For the photo-ionisation, we have included the radiative transfer effect following the simple recipe in Appendix of Kitayama & Ikeuchi (2001), who derive an analytical expression under the assumption of a power law spectrum of incident photons. For the spectral shape parameter α of the radiation field, we adopt $\alpha = 3$, because the resulting ratio between H_2 destroying photons and H ionizing photons is similar to realistic OB stars. Kitayama et al. (2001) have examined $\alpha = 1$ and $\alpha = 5$. Their table 1 indicates that $\alpha = 1$ overproduces the ionizing photons while $\alpha = 5$ overproduces the H_2 destroying photons. Therefore, we adopt an intermediate value: $\alpha = 3$. In any case, different values of α do not affect the behaviour of x , f_{H_2} , and T as functions of time, because the dust accumulation (which does not depend on α) is the greatest influence on these three quantities. The normalisation of the intensity, $I_0(\nu_{\text{HI}})$, is determined from

$$cu_{\text{UV}} \equiv \frac{L_{\text{UV}}}{(r_{\text{SF}}/2)^2} = 4\pi \int_{\nu_{\text{min}}}^{\infty} I_0(\nu_{\text{HI}}) \left(\frac{\nu}{\nu_{\text{HI}}} \right)^{-\alpha} d\nu, \quad (2)$$

where $\nu_{\text{min}} (\simeq 10^{15} \text{ Hz})$ is the minimum frequency where OB stars dominate the radiative energy, u_{UV} is the ‘‘typical’’ interstellar radiation field estimated at the half of the radius ($r_{\text{SF}}/2$; half is for a rough average), ν_{HI} is the ionisation frequency of neutral hydrogen ($\nu_{\text{HI}} = 3.3 \times 10^{15} \text{ Hz}$) (see HF02 for details), and c is the light speed.

In calculating f_{H_2} , we consider H_2 formation both in the gas phase (via H^- or H_2^+ , where the latter is negligible), and on the dust grain surface; H_2 destruction occurs through collisions with H^+ , H, and e^- , and photodissociation. For self-shielding effects which prohibit H_2 dissociation, equation (17) of HF02 is used, but here we substitute r_{disc} with $r_{\text{SF}}/2$. For the reaction rates, we adopt table 1 of HF02, but for the reaction on dust grains, R_{dust} , we use the following expression which includes the dependence on a :

$$R_{\text{dust}} = \begin{cases} 2.8 \times 10^{-15} \left(\frac{T}{100 \text{ K}} \right)^{1/2} \left(\frac{a}{0.03 \mu\text{m}} \right)^{-1} \\ \quad \times \left(\frac{\delta}{2 \text{ g cm}^{-3}} \right)^{-1} \text{ cm}^3 \text{ s}^{-1} \text{ if } T \leq 300 \text{ K} \\ 0 \text{ if } T > 300 \text{ K} \end{cases} \quad (3)$$

In order to calculate the temperature evolution, cooling and heating must be considered in our model. We assume that cooling processes comprise collisional excitation and ionisation of atomic hydrogen (when $T \gtrsim 8000 \text{ K}$) and collisional excitation of molecular hydrogen (which dominates for $T < 8000 \text{ K}$). For the heating by stellar UV radiation, we have included the radiative transfer ef-

fect by following a simple analytical recipe in Appendix of Kitayama & Ikeuchi (2000).

2.2. Star formation rate

Stars form as a result of the gravitational collapse of a gas cloud. Therefore, it is physically reasonable to relate the star formation rate with the free-fall timescale of gas. We consider a star-forming region with a gas number density of $n \sim n_{\text{H}}$. The free-fall time, t_{ff} , is estimated as

$$t_{\text{ff}} \simeq \frac{1}{\sqrt{G\rho}} \simeq 1 \times 10^7 \left(\frac{n_{\text{H}}}{100 \text{ cm}^{-3}} \right)^{-1/2} \text{ yr}, \quad (4)$$

where $\rho = m_{\text{H}}n_{\text{H}}$ (m_{H} is the mass of a hydrogen atom) is the mass density of the gas. The star formation rate, ψ , is estimated as

$$\begin{aligned} \psi &= \frac{\epsilon_{\text{SF}} M_{\text{gas}}}{t_{\text{ff}}} \Theta(t) \\ &\simeq 0.1 \left(\frac{\epsilon_{\text{SF}}}{0.1} \right) \left(\frac{M_{\text{gas}}}{10^7 M_{\odot}} \right) \left(\frac{n_{\text{H}}}{100 \text{ cm}^{-3}} \right)^{1/2} \Theta(t) \\ &M_{\odot} \text{ yr}^{-1}, \end{aligned} \quad (5)$$

where M_{gas} is the total gas mass (both molecular and atomic) of the star-forming region, ϵ_{SF} is the star formation efficiency defined as the conversion efficiency of a gas into stars over a free-fall time, and $\Theta(t)$ is Heaviside’s step function [$\Theta(t) = 1$ if $t \geq 0$ and $\Theta(t) = 0$ if $t < 0$]. Thus, we define the zero point of time t at the onset of star formation in the star-forming region. For simplicity, we assume a constant star formation rate (i.e., ϵ_{SF} , M_{gas} , and n_{H} are approximated to be constant) and a spherical homogeneous star forming region. In reality, there is probably a significant density inhomogeneity; however, the star formation rate in the entire star-forming region may be regulated by the dynamical time governed by a spatially averaged density, and the homogeneous density can be regarded as such an average.

The hydrogen number density can be related to gas mass as

$$\frac{4\pi}{3} r_{\text{SF}}^3 n_{\text{H}} m_{\text{H}} = M_{\text{gas}}, \quad (6)$$

where r_{SF} is the radius of the star-forming region. Thus, the numerical value of the number density is estimated as

$$n_{\text{H}} \simeq 100 \left(\frac{r_{\text{SF}}}{100 \text{ pc}} \right)^{-3} \left(\frac{M_{\text{gas}}}{10^7 M_{\odot}} \right) \text{ cm}^{-3}. \quad (7)$$

We also define the gas consumption timescale t_{gas} :

$$t_{\text{gas}} \equiv \frac{M_{\text{gas}}}{\psi} = \frac{t_{\text{ff}}}{\epsilon_{\text{SF}}}. \quad (8)$$

Since the effect of gas conversion into stars becomes significant for $t \sim t_{\text{gas}}$, we stop the calculation at $t = t_{\text{gas}}/2$. After this time, star formation may be suppressed because of the lack of gas.

2.3. Evolution of dust content

We calculate the evolution of dust mass in a star-forming region considering the dust supply from SNe II. The pre-existing dust at $t = 0$ in the star-forming region is neglected here. This is a good approximation for the extremely metal-poor BCDs treated in this paper. In fact, a large fraction of dust amount contained in some BCDs can be explained by the present star formation activity (see Section 3.3). Preexisting dust would strengthen all the dust effects described below.

If the starburst is young, and there has been no previous burst, dust can be supplied only from massive stars with short lifetimes. Thus, SNe II are the dominant source of dust formation if the age is typically less than a few times 10^8 yr (Dwek 1998). Thus, the dust formation rate is related to the rate of SNe II. The SN II rate as a function of time, $\gamma(t)$, is given by

$$\gamma(t) = \int_{8 M_{\odot}}^{\infty} \psi(t - \tau_m) \phi(m) dm, \quad (9)$$

where $\psi(t)$ is the star formation rate at t (Eq. 5), $\phi(m)$ is the initial mass function (IMF; the definition of the IMF is the same as that in Tinsley 1980), τ_m is the lifetime of a star whose mass is m , and we assume that only stars with $m > 8 M_{\odot}$ produce SNe II. In this paper, we assume a Salpeter IMF ($\phi(m) \propto m^{-2.35}$) with the stellar mass range of $0.1\text{--}60 M_{\odot}$ (HF02). If we assume a higher upper limit such as $100 M_{\odot}$, we expect a higher SN II rate and dust production rate. However, if the progenitor mass m is larger than $\sim 50 M_{\odot}$, almost all the produced metals may collapse into a central blackhole (Tsujiimoto et al. 1997). Todini & Ferrara (2001) treated only progenitor stellar mass less than $40 M_{\odot}$, and the dust production rate for massive stars ($\gtrsim 60 M_{\odot}$) is unknown theoretically. Recently, however, there have been some advances in this field (Nozawa et al. 2003; Schneider et al. 2004), and we are developing a model to include the effect of massive stars.

Dust destruction by shocks from SNe II can be important (Dwek & Scalzo 1980; Jones et al. 1996). The destruction timescale τ_{SN} is estimated to be (McKee 1989; Lisenfeld & Ferrara 1998)

$$\tau_{\text{SN}} = \frac{M_{\text{gas}}}{\gamma \epsilon_{\text{SN}} M_s}, \quad (10)$$

where M_s is the mass accelerated to a velocity large enough for dust destruction by a SN blast ($\sim 100 \text{ km s}^{-1}$), γ is the SN II rate, ϵ_{SN} is the efficiency of dust destruction in a medium shocked by a SN II. We adopt $M_s = 6.8 \times 10^3 M_{\odot}$ (Lisenfeld & Ferrara 1998; see also Tielens 1998) and $\epsilon_{\text{SN}} = 0.1$ (McKee 1989). Since we are interested in extremely metal-poor environments, we assume the relation between stellar mass and lifetime of zero-metallicity stars in table 6 of Schaerer (2002).²

² The case without mass loss is applied for consistency with HF02. This does not unduly affect our results however since

Dust grains can also be destroyed by strong and hard interstellar radiation fields (e.g., Boulanger et al. 1988; Puget & Léger 1989; Voit 1992; Contursi et al. 2000). However, the grain populations most strongly affected are the carriers of the aromatic band features (e.g., Polycyclic Aromatic Hydrocarbons) and very small grains (diameter $a < 0.01 \mu\text{m}$), neither of which are considered here. Hence, since grain destruction processes by UV radiation are most severe for very small grains, and in any case are poorly known, we will neglect them.

In this case the rate of increase of M_{dust} is written as

$$\frac{dM_{\text{dust}}}{dt} = m_{\text{dust}} \gamma - \frac{M_{\text{dust}}}{\tau_{\text{SN}}}, \quad (11)$$

where m_{dust} is the typical dust mass produced in a SN II. Todini & Ferrara (2001) show that m_{dust} varies with progenitor mass, metallicity (Z), and input energy of SNe II. The Salpeter IMF-weighted mean of dust mass produced per SN II for (1) $Z = 0$, Case A, (2) $Z = 0$, Case B, (3) $Z = 10^{-2} Z_{\odot}$, Case A, and (4) $Z = 10^{-2} Z_{\odot}$, Case B are (1) $0.22 M_{\odot}$, (2) $0.46 M_{\odot}$, (3) $0.45 M_{\odot}$, and (4) $0.63 M_{\odot}$, respectively (Z is the metallicity, and Cases A and B correspond to low and high explosion energy³ for Case A and Case B, respectively.) We adopt the average of the four cases, i.e., $m_{\text{dust}} = 0.4 M_{\odot}$ (HHF02). This may not be an overly optimistic estimate given the low upper mass cutoff of $35 M_{\odot}$ adopted by Todini & Ferrara (2001), and the higher dust production estimates of Nozawa et al. (2003). The calculated dust mass M_{dust} is roughly proportional to m_{dust} , and the timescale on which the dust extinction effects appear is approximately proportional to $1/m_{\text{dust}}$.

2.4. Evolution of metal content

The evolution of metal content can be calculated once the star formation history and metal yield are fixed (e.g., Tinsley 1980). Because of the young age range ($\lesssim 10^8$ yr) treated in this paper, we assume that the metal production is dominated by SNe II. The evolution of the mass of metals (a given species is indicated by i) in the gas phase, M_i , is calculated by subtracting the dust mass from the metal mass. This is expressed as

$$\frac{dM_i}{dt} = m_i \gamma - \frac{dM_{\text{dust}, i}}{dt}, \quad (12)$$

where m_i is the IMF-weighted average of metal mass (for species i) ejected per SN II and $M_{\text{dust}, i}$ is the mass of element i in dust phase. We calculate the abundances of carbon and oxygen, because those two elements are the two major metals produced in SNe II (Woolsey & Weaver 1995). Following HF02, we adopt $M_{\text{dust}, \text{O}} = 0.15 M_{\text{dust}}$, $M_{\text{dust}, \text{C}} = 0.36 M_{\text{dust}}$, $m_{\text{O}} = 1.2 M_{\odot}$, and $m_{\text{C}} = 0.17 M_{\odot}$; i.e., we assume that carbonaceous grains are responsible

the differences in metallicity and luminosity for the case *with* and *without* mass loss are within a factor of 2.

³ The kinetic energies given to the ejecta are 1.2×10^{51} erg and 2×10^{51} erg

for 36% of the total dust mass, and the other grains contain oxygen with mass fraction of 23% (i.e., the oxygen fraction in mass is $0.64 \times 0.23 = 0.15$).

2.5. Radiative properties

One of the most direct ways to constrain dust content is to observe IR continuum emission from dust grains. We now derive the evolution of IR luminosity. Because of the large cross section of grains against UV light and the intense UV interstellar radiation field in star-forming galaxies, we can assume that the IR luminosity is equal to the absorbed energy of UV light.

2.5.1. UV and IR

First, we estimate the fraction of the UV radiation absorbed by dust. We define the following typical optical depth, τ_{dust} , as

$$\tau_{\text{dust}} \equiv \pi a^2 Q_{\text{UV}} n_{\text{dust}} r_{\text{SF}} / 2. \quad (13)$$

where $\pi a^2 Q_{\text{UV}}$ is the typical absorption cross-section for UV light (Q_{UV} is the dimensionless absorption cross-section normalised by the geometrical cross-section), a is the dust radius, n_{dust} is the mean dust grain number density, and we assume that the typical path length for a UV photon is half of r_{SF} as a rough average.⁴ In this paper we assume for simplicity a single value for a , consistently with the typical size of dust grains produced by SNe II (e.g., Todini & Ferrara 2001; Nozawa et al. 2003). The dust mass density δ is related to the mean dust number density n_{dust} as

$$\frac{4\pi}{3} a^3 \delta n_{\text{dust}} \frac{4\pi}{3} r_{\text{SF}}^3 = M_{\text{dust}}, \quad (14)$$

where δ is the grain material density. By solving Eq. (14) for n_{dust} and substituting it into Eq. (13), we obtain

$$\tau_{\text{dust}} = \frac{9}{32\pi} \frac{Q_{\text{UV}} M_{\text{dust}}}{a \delta r_{\text{SF}}^2}. \quad (15)$$

We define the ‘‘attenuation function’’ $E(\tau_{\text{dust}})$ as the fraction of UV light escaping from the star-forming region. Thus, we write the UV luminosity of the star-forming region as

$$L_{\text{UV}} \simeq L_{\text{UV},0} E(\tau_{\text{dust}}), \quad (16)$$

where $L_{\text{UV},0}$ is the intrinsic UV luminosity. The functional form of $E(\tau_{\text{dust}})$ depends on the geometry of dust distribution, and we examine the following two representative simple cases. One is the ‘‘screen’’ distribution, in which all the dust is located at the radius of r_{SF} from the centre of

the star-forming region. The other is the ‘‘mixed’’ geometry, in which the spatial distributions of dust and stars are the same (i.e., the mass ratio between stars and dust is constant). In the screen geometry,

$$E(\tau_{\text{dust}}) = E_{\text{sc}}(\tau_{\text{dust}}) \equiv \exp(-\tau_{\text{dust}}), \quad (17)$$

while in the mixed geometry,

$$E(\tau_{\text{dust}}) = E_{\text{mix}}(\tau_{\text{dust}}) \equiv [1 - \exp(-\tau_{\text{dust}})] / \tau_{\text{dust}}. \quad (18)$$

Since $E_{\text{mix}} > E_{\text{sc}}$ for a given τ_{dust} , the screen geometry shields the UV light more efficiently. Moreover, the exponential behaviour of E_{sc} results in a strong cut-off of UV light at a certain time when a significant amount of dust is accumulated, while $E_{\text{mix}} \sim 1/\tau_{\text{dust}}$ for $\tau_{\text{dust}} \gg 1$, which means that UV light originating from the ‘‘surface’’ always escapes. We do not treat a clumpy dust distribution, since inhomogeneity changes average optical depths in ways that depend on the specific geometry (Natta & Panagia 1984); such a treatment is beyond the scope of this paper.

$L_{\text{UV},0}$ is assumed to be equal to the total luminosity of OB stars, whose mass is larger than $3 M_{\odot}$ (Cox 2000):

$$L_{\text{UV},0}(t) = \int_{3 M_{\odot}}^{\infty} dm \int_0^{\tau_m} dt' L(m) \phi(m) \psi(t - t'), \quad (19)$$

where $L(m)$ is the stellar luminosity as a function of stellar mass (m). This UV luminosity is also used in Eq. (16) to estimate the UV luminosity L_{UV} after the dust absorption, and the same L_{UV} is also in Eq. (2). For $L(m)$, we adopt the model of zero-metallicity stars without mass loss in Schaerer (2002). Assuming that all the absorbed energy is reemitted in the IR, the IR luminosity L_{IR} becomes:

$$L_{\text{IR}} = L_{\text{UV},0} - L_{\text{UV}} = L_{\text{UV},0} [1 - E(\tau_{\text{dust}})]. \quad (20)$$

2.5.2. Dust temperature

Another important quantity representative for the radiative properties of a star-forming region is dust temperature. The equilibrium dust temperature is determined from the balance between incident radiative energy and radiative cooling. The equilibrium temperature is expressed as follows (Takeuchi et al. 2003):

$$T_{\text{dust}} \simeq \left(\frac{hc}{\pi k} \right) \left\{ \frac{63 u_{\text{UV}} Q_{\text{UV}}}{64 \pi (2\pi A a) hc} \right\}^{1/6}, \quad (21)$$

where the UV radiation field is calculated by Eq. (2) and the dimensionless dust emissivity in the IR is assumed to satisfy⁵

$$Q_{\text{IR}}(a, \lambda) = \frac{2\pi A a}{\lambda^2}. \quad (22)$$

For silicate grains $A = 1.34 \times 10^{-3}$ cm (Drapatz & Michel 1977), while for carbonaceous grains $A = 3.20 \times 10^{-3}$ cm

⁵ Strictly speaking, this is valid for $\lambda \gtrsim 20 \mu\text{m}$ for silicate grains, and $\lambda \gtrsim 50 \mu\text{m}$ for carbonaceous ones.

⁴ In order to fully derive the precise path length instead of roughly dividing r_{SF} by 2, a detailed modelling of radiative transfer including dust scattering is necessary. Here we only mention that with a given dust mass, τ_{dust} linearly scales with the adopted path length.

(Draine & Lee 1984; Takeuchi et al. 2003). The derivation of Eq. (21) is found in the Appendix. The numerical expression for T_{dust} is

$$T_{\text{dust}} = 14.6 \left(\frac{u_{\text{UV}}}{4.0 \times 10^{-14} \text{ erg cm}^{-3}} \right)^{1/6} \times \left(\frac{A}{3.2 \text{ cm} \times 10^{-3}} \right)^{-1/6} \left(\frac{a}{0.03 \text{ } \mu\text{m}} \right)^{-1/6} \times Q_{\text{UV}}^{1/6} \text{ K}, \quad (23)$$

where we explicitly express the dependence on a . The equilibrium dust temperature is seen to be rather insensitive to changes in the input parameters. We adopt $A = 3.2 \times 10^{-3}$ cm since that is the grain radius appropriate for graphites (Todini & Ferrara 2001). With this value, we obtain

$$Q_{\text{IR}}(a, \lambda) = 6.03 \times 10^{-4} \left(\frac{a}{0.03 \text{ } \mu\text{m}} \right) \left(\frac{\lambda}{100 \text{ } \mu\text{m}} \right)^{-2}. \quad (24)$$

For a grain size of $0.03 \text{ } \mu\text{m}$ (carbonaceous grains), and a density $\delta = 2 \text{ g cm}^{-3}$ (Draine & Lee 1984), this corresponds to the following value of dust mass-absorption coefficient, $\kappa_{\nu} (\equiv 3Q_{\text{IR}}/4a\delta)$ (Hildebrand 1983):

$$\kappa_{\nu} = 75 \left(\frac{\lambda}{100 \text{ } \mu\text{m}} \right)^{-2} \left(\frac{\delta}{2 \text{ g cm}^{-3}} \right)^{-1} \text{ cm}^2 \text{ g}^{-1}. \quad (25)$$

Although there is little observational constraint on Q_{IR} and κ_{ν} of dust produced by SNe II, we can compare our κ_{ν} with the data of Galactic or extragalactic observations. At $\lambda = 850 \text{ } \mu\text{m}$, $\kappa_{\nu} \simeq 1.0 \text{ cm}^2 \text{ g}^{-1}$, while observational data suggest $\kappa_{\nu} \simeq 0.7\text{--}2.4 \text{ cm}^2 \text{ g}^{-1}$ (Alton et al. 2001; James et al. 2002). Bianchi et al. (1999) find that Q_{IR} around $\lambda = 100 \text{ } \mu\text{m}$ is roughly $\sim 10^{-3}\text{--}5 \times 10^{-4}$ if we assume Q at V band is ~ 1 (see also Fig. 5 of James et al. 2002 and references therein).

2.6. Initial conditions

For the onset of star formation, the gas must be cool. The molecular hydrogen cooling eventually cools gas down to $T \sim 300 \text{ K}$ (e.g., Tegmark et al. 1997). During the phase of efficient molecular formation in gas, the ionisation fraction x is roughly $\sim 10^{-4}$ and the molecular fraction is $f_{\text{H}_2} \sim 10^{-3}$. After this phase, the ionisation degree x decreases and the gas phase reaction stops. Since stars begin to form during molecular formation, we set the initial values as $x = 10^{-4}$, $T = 300 \text{ K}$, and $f_{\text{H}_2} = 10^{-3}$. However, the gas starts to be ionised and the molecules begins to dissociate soon ($< 1 \text{ Myr}$) after the onset of star formation, and the results do not depend strongly on the initial conditions for x and f_{H_2} . The initial temperature does not change the evolution of gas as long as $T \lesssim 10^3 \text{ K}$ initially.

2.7. Selection of parameters

For the UV light, because of the short wavelength, we can assume that $Q_{\text{UV}} \simeq 1$. For the grain radius, we examine

the following two cases: small dust ($a = 0.03 \text{ } \mu\text{m}$) proposed by Todini & Ferrara (2001), and large dust ($a = 0.1 \text{ } \mu\text{m}$) possibly produced even in SNe II (Nozawa et al. 2003). We fix $m_{\text{dust}} = 0.4 M_{\odot}$ (Section 2.3), and adopt $\delta \simeq 2 \text{ g cm}^{-3}$ (Draine & Lee 1984). As mentioned in Section 2.3, the timescale of dust effects (enhancement of molecular content, enhancement of UV shielding, etc.) is roughly inversely proportional to m_{dust} .

The free parameters which remain to be determined are r_{SF} , M_{gas} , and ϵ_{SF} . Since our aim is to investigate the properties of “active” and “passive” star-forming regions, which correspond to compact and diffuse regions, respectively, we should examine various r_{SF} . In order to concentrate on the effect of compactness, the gas mass is fixed. A representative value for a star-forming region in BCDs can be taken as $M_{\text{gas}} = 10^7 M_{\odot}$. This is a typical value for gas masses derived for star-forming regions in SBS 0335–052 and IZw 18 representative extremely metal-poor BCDs (Section 4.2). In order to concentrate on the variation of r_{SF} , we therefore fix $M_{\text{gas}} = 10^7 M_{\odot}$, and examine a region size range typical of BCDs: $r_{\text{SF}} = 30 \text{ pc}$, 100 pc , and 300 pc , corresponding to the density $n \sim 3000 \text{ cm}^{-3}$, 100 cm^{-3} , and 3 cm^{-3} , respectively, with $M_{\text{gas}} = 10^7 M_{\odot}$. The most compact case is representative of the “active” class, while the most diffuse case is typical of the “passive” class.

The remaining free parameter is the star formation efficiency ϵ_{SF} , which we assign a value $\epsilon_{\text{SF}} = 0.1$ (e.g., Ciardi et al. 2000; Ferrara et al. 2000; Inoue et al. 2000; Barkana 2002; Scannapieco et al. 2003; Salvaterra & Ferrara 2003) unless otherwise stated. Roughly speaking, the timescale on which the dust effects appear scales inversely with ϵ_{SF} . For example, the rapid increase of molecules and drop of temperature appear on a timescale proportional to $1/\epsilon_{\text{SF}}$. It is possible that ϵ_{SF} may change significantly as a function of time, but our simple assumption of constant ϵ_{SF} is a useful first-order approximation. ϵ_{SF} and the star formation rate should be regarded as an average over the timescale in which we are interested. High and low star formation efficiencies are investigated in the models of IZw 18 and SBS 0335–052 in Section 4.2.

These values are all representative of metal-poor star-forming regions. Typically, BCDs have $\psi \sim 0.01\text{--}1 M_{\odot} \text{ yr}^{-1}$, $r \sim 0.1\text{--}3 \text{ kpc}$ and $n \sim 10\text{--}1000 \text{ cm}^{-3}$ (Popescu et al. 1999; Hopkins et al. 2002).

3. Results

Here we illustrate the results for the time evolution of star-forming regions. First we adopt $a = 0.03 \text{ } \mu\text{m}$ and the screen dust distribution. Then, in Section 3.4, we investigate the dependence on grain size by assuming larger grains ($a = 0.1 \text{ } \mu\text{m}$) and on geometry by examining the effects of a mixed dust distribution (Eq. 18).

For continuous star-forming activity, the gas should continue to collapse. With a fixed density, the typical mass for the collapse, i.e., the Jeans mass, is determined by the gas temperature. Therefore, the evolution of the gas tem-

perature is one of the most important processes for understanding the fate of a star-forming region. In the following, we show the time evolution of gas temperature (T) and molecular fraction (f_{H_2}) for various region radii. Because we have assumed fixed values for M_{gas} , the density n_{H} is thus determined by setting r_{SF} . Moreover, since we have also fixed ϵ_{SF} , the resulting star-formation rate ψ , given by Eq. (5), also depends on r_{SF} through the density n dependence.

3.1. Gas state

In Fig. 1, we show the evolution of (a) gas temperature, (b) ionisation degree, and (c) molecular fraction for $r_{\text{SF}} = 30, 100, 300$ pc (solid, dotted, and dashed lines, respectively). We stop our calculation at $t = t_{\text{gas}}/2$, when our assumption that M_{gas} is constant becomes invalid (see Eq. 8). Therefore the lines are truncated at 8 Myr and 50 Myr for $r_{\text{SF}} = 30$ pc and 100 pc, respectively. We observe that as the region size becomes smaller (i) the gas remains cooler, (ii) the ionisation degree remains lower, and (iii) the molecular fraction increases more rapidly.

In the time evolution of these three parameters, accumulation of dust grains plays a fundamental role. The dust accumulation in a compact region results in a large optical depth and a large density of dust grains. As a result, the molecular formation tends to increase rapidly, because of the large density of dust grains and the consequent large shielding of dissociating photons. Since the UV photons are efficiently shielded by dust grains, the gas is kept cool and the ionisation degree remains low.

The temporal behaviour of the molecular fraction is explained as follows (see Fig. 1c). The first drastic increase of the molecular fraction, seen around 4 and 13 Myr for $r_{\text{SF}} = 30$ and 100 pc, respectively, is due to the activation of the gas-phase reactions caused by the increase of ionisation degree and the temperature drop. The molecular formation is suppressed for $r_{\text{SF}} = 300$ pc because the gas temperature remains high $\sim 10^4$ K. The second drastic increase of the molecular fraction, seen around 5 and 20 Myr for $r_{\text{SF}} = 30$ and 100 pc, respectively (for $r_{\text{SF}} = 300$ pc, the second increase is not before 100 Myr), is due to the onset of molecule formation on dust grains: dust grains shield the ionising photons and facilitate the gas cooling down to 300 K. At this temperature, the H_2 formation on dust grains becomes possible. For $r_{\text{SF}} = 300$ pc, representative of the passive mode, H_2 formation occurs only in the gas phase with a low reaction rate because of the high gas temperature.

3.2. Luminosities

To see how much UV light is shielded by dust, we show the evolution of IR and UV luminosities in Fig. 2a for $r_{\text{SF}} = 30$ pc and $r_{\text{SF}} = 300$ pc, corresponding to the active and passive modes, respectively. We see that the IR vs. UV luminosity ratio increases more rapidly in the com-

compact ($r_{\text{SF}} = 30$ pc) region than in the diffuse ($r_{\text{SF}} = 300$ pc) one. This is due to the large dust optical depth in compact star-forming regions. The efficient shielding of UV in compact regions also keeps the molecular fraction high since UV dissociation is suppressed.

The evolution of dust temperature determined from Eq. (23) is also shown in Fig. 2b for $r_{\text{SF}} = 30$ pc and 300 pc. The lines start from the onset of the first SNe II (i.e., $t = 3$ Myr), when dust production begins. The dust temperature is initially ~ 100 K and decreases rapidly for the compact “active” case. This rapid decrease is due to the strong shielding of UV light by dust grains. The dust temperature remains ~ 50 K for the “passive” case.

3.3. Chemical enrichment

In order to ascertain if our chemical enrichment model is capable of explaining the observed metallicities, we calculate the evolution of oxygen abundance. Since the optical oxygen emission lines from ionised regions are often used as a tracer of chemical abundance (e.g., Izotov & Thuan 1999), we calculate the evolution of oxygen mass (see Section 2.4); the solar abundance is assumed to correspond to $M_{\text{O}}/M_{\text{gas}} = 0.01$ (Cox 2000), where M_{gas} is assumed to be constant in time. Fig. 3a shows the evolution of $[\text{O}/\text{H}]$ for the three region radii depicted in Fig. 1. The metallicity of the 30-pc region reaches 1/50 solar in 7 Myr. Not surprisingly, the metal enrichment in diffuse regions proceeds more slowly: in particular, the 300-pc region is enriched to 1/50 solar in ~ 30 Myr.

The evolution of dust-to-gas ratio ($\mathcal{D} \equiv M_{\text{dust}}/M_{\text{g}}$) is shown in Fig. 3b. We have assumed that the star-forming regions contain no dust and metals initially. This assumption holds if a large part of the present dust and metals is supplied during the present episode of star formation. This assumption is adopted based on the picture that BCDs are relatively young galaxies whose major star formation episodes have occurred quite recently ($\lesssim 100$ Myr; e.g., Tomita et al. 2002; Takeuchi et al. 2004). This point will be further discussed when we compare our model with the observational properties of BCDs (Section 4.2).

3.4. Grain size and distribution geometry

Nozawa et al. (2003) have recently pointed out that grains larger than predicted by Todini & Ferrara (2001) can form even in SNe II. Grains may be as large as $a \sim 0.1 \mu\text{m}$, and therefore, we also examine this case.

In order to evaluate the effect of shielding, we show the evolution of UV and IR luminosities for $a = 0.1 \mu\text{m}$ with the screen geometry in Fig. 4a. With a fixed dust mass, the dust optical depth against the UV photons, τ_{dust} , is proportional to a^{-1} , because $n_{\text{dust}} \propto a^{-3}$ and $\tau_{\text{dust}} \propto a^2 n_{\text{dust}}$ (Eq. 13). Therefore, if the grain size is larger, more UV radiation escapes without being absorbed by dust grains. Consequently, the IR luminosity becomes dominant relative to L_{UV} later for $a = 0.1 \mu\text{m}$ than for $a = 0.03 \mu\text{m}$,

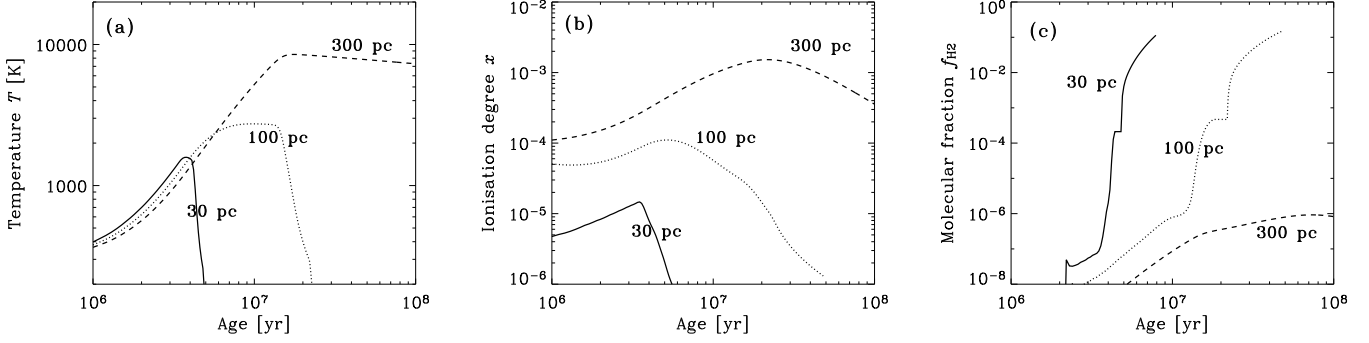


Fig. 1. Time evolution of **a)** gas temperature, **b)** ionisation degree, and **c)** molecular fraction for various radii of the star-forming region (solid, dotted, and dashed lines for $r_{\text{SF}} = 30$ pc, 100 pc, and 300 pc, respectively). The gas mass and the star formation efficiencies are assumed to be $1.0 \times 10^7 M_{\odot}$ and 0.1, respectively.

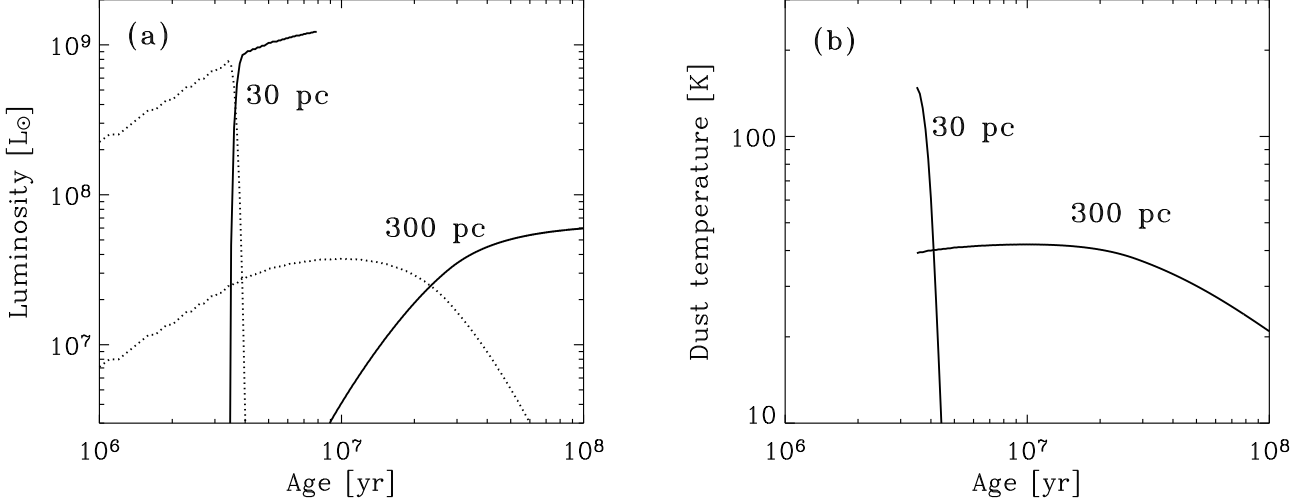


Fig. 2. **a)** Time evolution of IR and UV luminosities (solid and dotted lines, respectively). The left lines are for the compact ($r_{\text{SF}} = 30$ pc) case and the right lines are for diffuse ($r_{\text{SF}} = 300$ pc) case. The gas mass is assumed to be $10^7 M_{\odot}$ (same as Fig. 1). **b)** Time evolution of dust temperature. The upper and lower lines are for $r_{\text{SF}} = 30$ pc and $r_{\text{SF}} = 300$ pc, respectively. The lines start from the age of around 3 Myr, when dust begins to be produced. The screen dust distribution and the small dust grain ($a = 0.03 \mu\text{m}$) are assumed for both panels.

although the difference is not significant especially for the compact ($r_{\text{SF}} = 30$ pc) region. For $r_{\text{SF}} = 30$ pc, the IR luminosity dominates as soon as the dust production begins (~ 3 – 4 Myr).

We also show the evolution of dust temperature in Fig. 4b. The dust temperature drops rapidly in compact regions ($r_{\text{SF}} = 30$ pc) because of the efficient shielding of UV radiation. For diffuse regions ($r_{\text{SF}} = 300$ pc), the temperature drop relative to small grains is not significant because the shielding is inefficient. Owing to the $a^{-1/6}$ dependence of dust temperature (Eq. 23), the dust temperature is lower for $a = 0.1 \mu\text{m}$ than $a = 0.03 \mu\text{m}$.

Next, in order to investigate the effect of dust distribution geometry, we examine the mixed geometry using the attenuation function expressed in Eq. (18) rather than Eq. (17). The evolution of UV and IR luminosities

is shown in Fig. 5a. The UV light decreases more mildly in the mixed geometry than with the screen geometry, because UV light originating from the “surface” of star-forming regions always escapes as described in Section 2.5.1. The evolution of dust temperature is shown in Fig. 5b. We see that the strong “exponential” drop of dust temperature with the screen geometry (Figs. 2b and 4b) is not seen in the mixed case because of the milder shielding of UV light.

The physical state of the gas is also affected by the assumptions about dust grains. In order to clarify this point, we compare the evolution of gas temperature, ionisation degree, and molecular fraction in Fig. 6 for the case of $r_{\text{SF}} = 100$ pc. The solid lines, which are the same as the dotted lines in Fig. 1, show the case of $a = 0.03 \mu\text{m}$ and the screen geometry (called “standard”). The dotted and

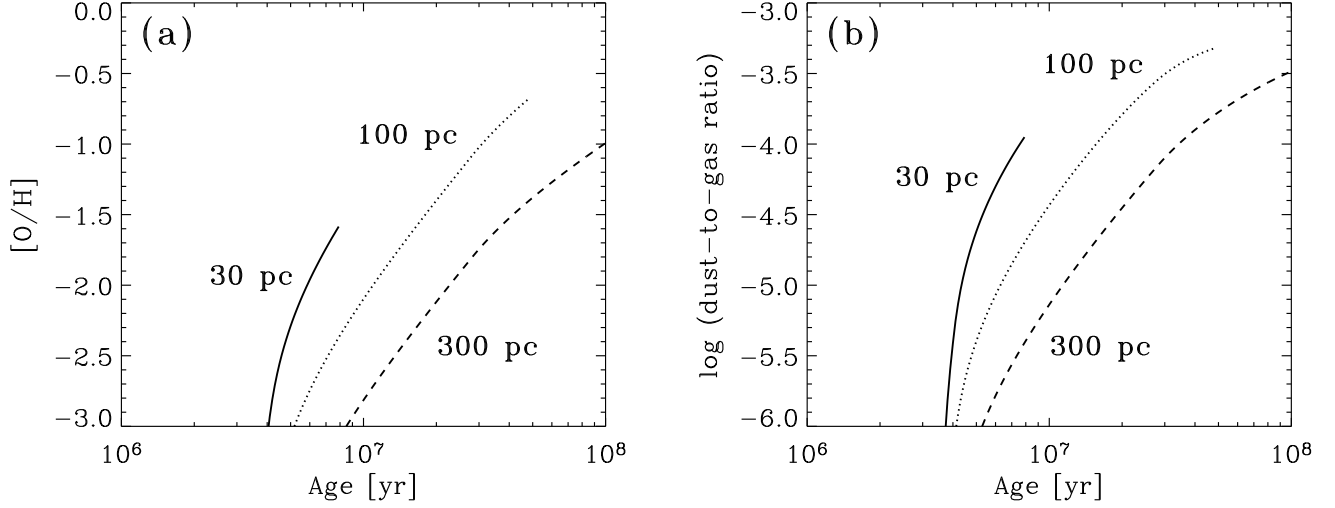


Fig. 3. Time evolution of oxygen abundance in gas phase. $[O/H]$ is the oxygen abundance in logarithmic scaling, where $[O/H] = 0$ is the solar oxygen abundance. The solid, dotted, and dashed lines are for $r_{SF} = 30$ pc, 100 pc, and 300 pc, respectively. The gas mass and the star formation efficiency are assumed to be $10^7 M_{\odot}$ and 0.1, respectively (same as Fig. 1).

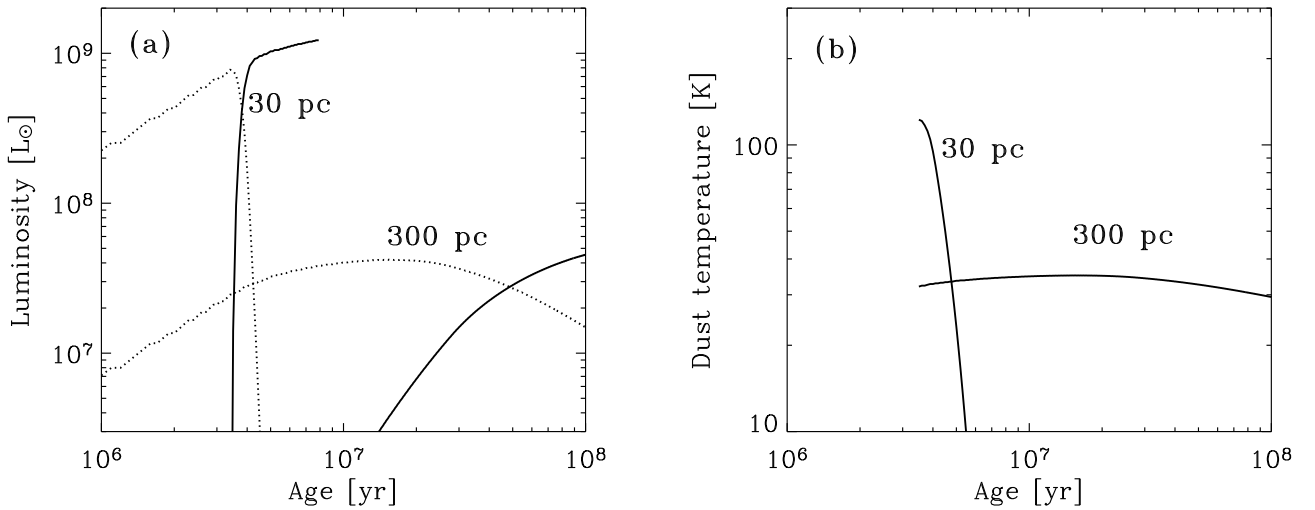


Fig. 4. **a)** Same as Fig. 2a, but for large grains ($a = 0.1 \mu\text{m}$). **b)** Same as Fig. 2b, but for large grains.

dashed lines represent the cases of the mixed geometry (with $a = 0.03 \mu\text{m}$) and $a = 0.1 \mu\text{m}$ (with the screen geometry). Because the UV optical depth of dust grains becomes smaller as the grain size increases, the heating and dissociation rates are larger for larger grains, which explains the behaviour of the dashed lines. For the molecular fraction, the formation rate on dust grains (Eq. 3) decreases because of the reduced dust surface, which also contributes to the slow increase of f_{H_2} for the larger grains. In the mixed geometry, the shielding of UV light is inefficient; the gas is heated and molecules are dissociated. Therefore, we conclude that the grain size and distribution are important to determine the physical state of gas.

To further investigate the effect of dust size and spatial distribution on our model results, we are planning to extend our study to include infrared SEDs. The study of SEDs has the advantage of being able to treat the multi-temperature, multi-size grain distributions, as well as stochastically heated grains (Takeuchi et al. 2003; see also Galliano et al. 2003). Not only extragalactic studies but also Galactic studies will help us understand why H_2 formation is enhanced in actively star-forming regions (e.g., Habart et al. 2003).

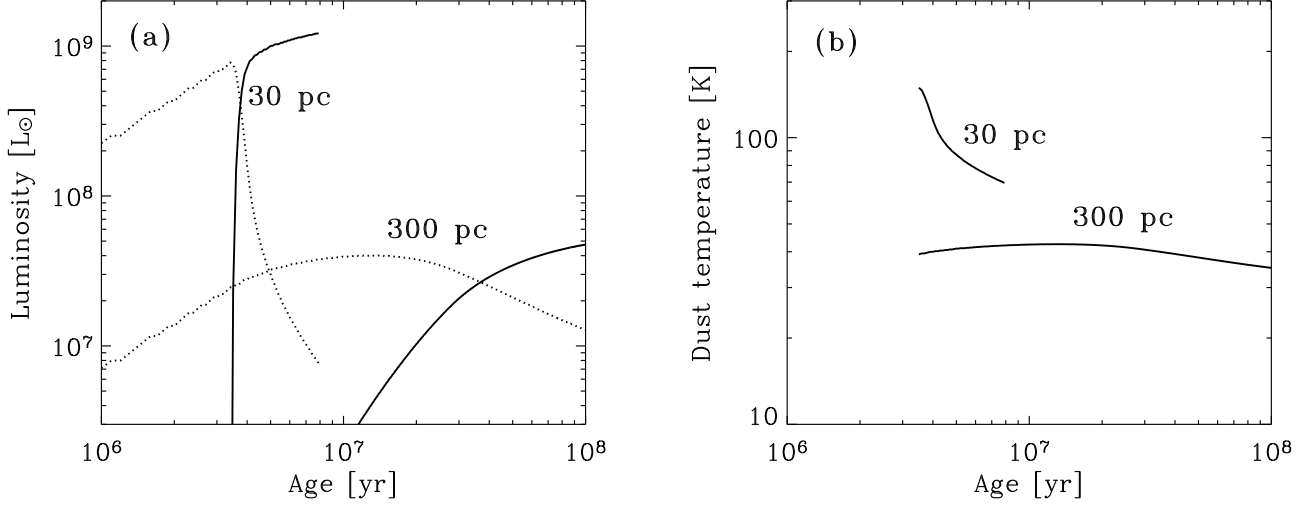


Fig. 5. **a)** Same as Fig. 2a, but for the mixed geometry of dust distribution. **b)** Same as Fig. 2b, but for the mixed geometry of dust distribution.

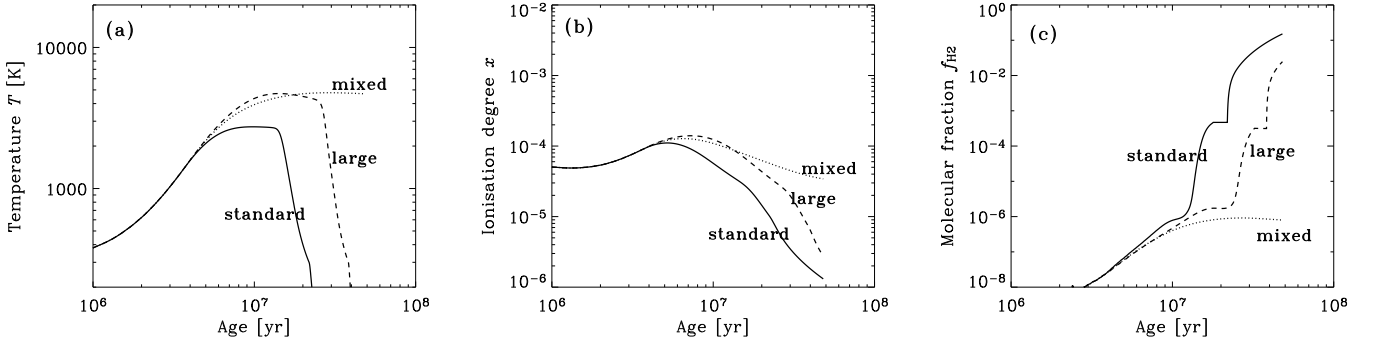


Fig. 6. Time evolution of **a)** gas temperature, **b)** ionisation degree, and **c)** molecular fraction for $r_{\text{SF}} = 100$ pc and $M_{\text{gas}} = 10^7 M_{\odot}$. The solid, dotted, and dashed lines represents the “standard” ($a = 0.03 \mu\text{m}$ and screen geometry) case, the mixed dust geometry ($a = 0.03 \mu\text{m}$), and the large dust grains of the star-forming region (solid, dotted, and dashed lines for $r_{\text{SF}} = 30$ pc, 100 pc, and 300 pc, respectively). The gas mass and the star formation efficiencies are assumed to be $1.0 \times 10^7 M_{\odot}$ and 0.1, respectively.

4. Active and passive BCDs

4.1. Physical properties

In the above, we have shown that both compact and diffuse star-forming regions can keep the ISM cool and rich in molecules. A compact and dense (typically $n \gtrsim 10^3 \text{ cm}^{-3}$, $r_{\text{SF}} \lesssim 50$ pc, and $\psi \gtrsim 0.1 M_{\odot} \text{ yr}^{-1}$) region forms stars on a timescale of $\lesssim 10$ Myr. This regime is termed an “active” mode in HHTIV. Since grains supplied by SNe II efficiently shield UV photons, the gas cools and molecule formation is enhanced. This implies that in such an active region, gas continues to collapse and stars form in a “run-away” mode. On the contrary, if a star-forming region is diffuse ($n \lesssim 50 \text{ cm}^{-3}$ and $r_{\text{SF}} \gtrsim 100$ pc), the star formation takes place “quiescently” ($\psi \lesssim 0.07 M_{\odot} \text{ yr}^{-1}$) on a timescale of $\gtrsim 10^8$ yr. This mode is called a “passive” mode in HHTIV. The latter regime inhibits an “active”

mode for the following two reasons: first, the gas collapse occurs slowly because of a long dynamical timescale; second, because of the inefficient shielding, it is subject to strong UV heating and photodissociation of molecules resulting from the star formation activity.

Let us consider our results from the viewpoint of the gas state. In an active region, independently of the initial conditions, the efficient dust accumulation lets the gas cool to $T \lesssim 300$ K through molecular cooling and UV shielding. Such a low temperature is crucial for the efficient formation of H_2 (Cazaux & Tielens 2002), causing a rapid increase of f_{H_2} . On the contrary, the evolution of a passive region proceeds without molecular cooling and UV shielding, and remains hotter ($T \gtrsim 5000$ K). This implies that the gravitational collapse in diffuse regions is inefficient and *self-regulated*, because of the stellar heat-

ing, especially the photo-ionisation heating (Lin & Murray 1992).

What determines the size and density of a star-forming region? With a constant density, the typical length of a gravitationally bound region is given by the Jeans length λ_J :

$$\lambda_J = 100 \left(\frac{T}{10^4 \text{ K}} \right)^{1/2} \left(\frac{n}{100 \text{ cm}^{-3}} \right)^{-1/2} \text{ pc}. \quad (26)$$

If a star-forming region is photo-heated, the gas temperature becomes $T \sim 10^4 \text{ K}$. Therefore, the typical size of a self-regulated star-forming region is determined by the gas density as $\sim 100(n/100 \text{ cm}^{-3})^{-1/2}$, consistent with the size of passive star-forming regions. Since an active star-forming region further cools through dust shielding, the gas collapses. We suggest that this collapse finally produces the high surface brightness and compact size observed for active star-forming regions.

Therefore, the initial gas density, which determines the self-gravitating length (Eq. 26) of a star-forming region, is important for the bifurcation into active and passive regimes. However, ambient pressure can also influence the fate of a star-forming region (e.g., Elmegreen & Efremov (1997; Elmegreen & Elmegreen 1997 Elmegreen & Hunter 2000) . Elmegreen & Efremov (1997) stress that the star formation efficiency is affected by ambient pressure. Shock compression may be important to create high-pressure environments (Elmegreen & Elmegreen 1997). A high pressure environment favours the formation of SSCs (Bekki & Couch 2001; Billett et al. 2002), which are observationally known to be associated with strong starbursts (e.g., Hunter et al. 1994). If a star-forming region is confined by a high environmental pressure, the compression of gas can lead to a high density and a short free-fall time. This means that high pressure regions tend to engender an active mode of star formation. Since there is no reason why the ambient pressure should be related to metallicity, this naturally explains why metallicity is not a primary factor of distinguishing active and passive modes.

To link ambient pressure and region size, it is appropriate to utilise the Ebert-Bonnor formalism for self-gravitating, pressure-bounded isothermal spheres (Ebert 1955; Bonnor 1956). The relation indicates that if r_{SF} is smaller than the critical radius,

$$\begin{aligned} r_c &= 0.49 \frac{kT}{m_H} \left(\frac{1}{Gp_{\text{ext}}} \right)^{1/2} \\ &= 43 \left(\frac{T}{10^4 \text{ K}} \right) \left(\frac{nT}{10^6 \text{ cm}^{-3} \text{ K}} \right)^{-1/2} \text{ pc}, \end{aligned} \quad (27)$$

the region becomes unstable and collapses. Therefore, if the region is compressed roughly down to $2r_c \sim 100 \text{ pc}$, it becomes unstable, and can evolve into an active star-forming region. Another important role of ambient pressure is to avoid the expansion of the star-forming region and to maintain a high-density environment. In summary, ambient pressure has two effects: one is to make the star-forming region gravitationally unstable, and the other is

to keep the density high which leads to short free-fall times (e.g., Elmegreen 2000).

4.2. Two prototypes

One of our main motivations is to clarify the reason why SBS 0335–052 and IZw 18 show different modes of star formation: active and passive (HHTIV). First, we “simulate” these two galaxies with our models. The necessary quantities for our model are M_{gas} and r_{SF} . The H I gas mass has been observationally derived as $\sim 10^9 M_{\odot}$ (Pustilnik et al. 2001) and $2.6 \times 10^7 M_{\odot}$ (van Zee et al. 1998) for SBS 0335–052 and IZw 18, respectively. However, we should consider these values as upper limits for M_{gas} , since M_{gas} is the gas mass in the star-forming regions, not in the entire system. It is difficult to resolve the star-forming regions in BCDs because they are generally small. On the other hand, typical gas densities in star-forming regions have been derived from the argument of collisional excitation based on high (spatial) resolution spectroscopy (e.g., Izotov et al. 1999). Although this argument is biased toward the ionised region close to massive stars, the gas density derived in this method can be considered to be representative of the entire star-forming region. Therefore, we will attempt to distinguish active and passive star formation and constrain the gas mass M_{gas} on the basis of observed region sizes r_{SF} (e.g., HHTIV) and gas densities.

4.2.1. IZw 18

We adopt $r_{\text{SF}} = 100 \text{ pc}$ and $n = 110 \text{ cm}^{-3}$ (Izotov et al. 1999; HHTIV). Eq. (7) indicates $M_{\text{gas}} \simeq 1 \times 10^7 M_{\odot}$ which is close to the M_{gas} estimated by van Zee et al. (1998). The free-fall time become $t_{\text{ff}} \sim 10 \text{ Myr}$ (Eq. 4). The observational star formation rate is $\sim 0.04\text{--}0.1 M_{\odot} \text{ yr}^{-1}$ (e.g., Hopkins et al. 2002). This range of star formation rate is consistent with Eq. (5) if we assume $\epsilon = 0.04\text{--}0.1$; we adopt $\epsilon = 0.07$ as a rough central value. In Fig. 7, we show the evolution of various physical quantities typical of IZw 18 by dotted lines. The shielding of UV photons by dust at $t \gtrsim 20 \text{ Myr}$ causes the efficient cooling, recombination, and molecular formation. In particular, if the age of IZw 18 is $\lesssim 20 \text{ Myr}$, the poor molecular content is consistent with observations (e.g., Vidal-Madjar et al. 2000).

Kamaya & Hirashita (2001) suggest that H_2 formation in IZw 18 may be regulated by the gas phase reaction, rather than by the formation on dust surfaces. If we assume the age of the youngest burst in IZw 18 to be $\sim 10 \text{ Myr}$, our calculation gives an ionisation fraction of $\sim 10^{-3}$, roughly consistent with Kamaya & Hirashita (2001). The molecular fraction is $\sim 10^{-6}$, consistent also with the upper limit by Vidal-Madjar et al. (2000).

Recchi et al. (2002) have proposed two instantaneous bursts separated by a quiescent period for IZw 18. The age of the recent burst deduced by them (4–15 Myr) is in

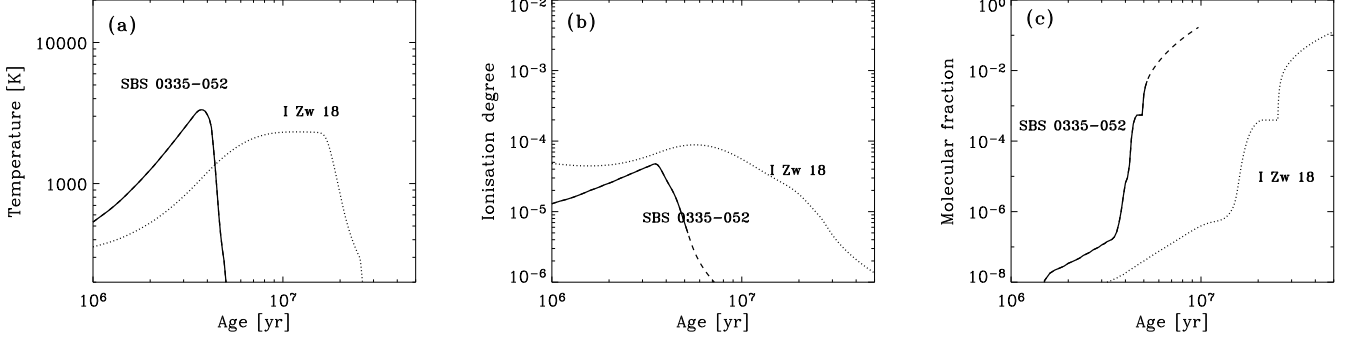


Fig. 7. Time evolution of **a)** gas temperature, **b)** ionisation degree, and **c)** molecular fraction for the model of SBS 0335–052 and I Zw 18 (solid and dotted lines, respectively). The dashed line continuing from the solid line shows the evolution after $t_{\text{gas}}/2$, when more than half of the initial gas mass is converted into stars.

the range treated in our paper, but an older burst which occurred ~ 300 Myr is probably also necessary (see also Aloisi et al. 1999; Östlin 2000). Hunt et al. (2003b) also derive a young burst age of 3–15 Myr, and a previous episode of star formation no older than $\lesssim 500$ Myr. However, the stars with the age $\lesssim 10$ Myr contribute to the gas heating more than the old stars, and therefore, the age in our model should be taken as the age of the more recent burst.

In Fig. 8, we present the evolution of oxygen abundance and dust-to-gas ratio for the model of I Zw 18 (dotted lines). The horizontal dash-dotted line represents the metallicity level observed for I Zw 18 (1/50 solar). This metallicity is reached at the age of ~ 20 Myr, which is roughly consistent with the above ages for the current star formation activity. At this age, the dust-to-gas ratio becomes 10^{-4} . The observational constraint on the dust-to-gas ratio is difficult at the moment, since we must specify the gas mass contained in star-forming regions, which are generally small for BCDs, and thus difficult to resolve. Nevertheless, we estimate for I Zw 18 $M_{\text{gas}} \simeq 1 \times 10^7 M_{\odot}$, on the same order of the $2.7 \times 10^7 M_{\odot}$ found by van Zee et al. (1998). The dust mass of I Zw 18 is in the range of $2\text{--}5 \times 10^3 M_{\odot}$ (Cannon et al. 2002). Therefore, we obtain a dust-to-gas ratio $\sim 10^{-4}$, which is roughly consistent with the model calculation at the age of ~ 20 Myr.

4.2.2. SBS 0335–052

The gas number density is roughly $n \sim 10^3 \text{ cm}^{-3}$ (Izotov et al. 1999; Hunt et al. 2004a), and the radius is $r_{\text{SF}} \sim 40$ pc. Eq. (7) indicates that $M_{\text{gas}} \sim 10^7 M_{\odot}$. The free-fall time is estimated to be $t_{\text{ff}} \sim 3$ Myr (Eq. 4). In order to be consistent with our previous paper, HHF02 ($\psi = 1 M_{\odot}$), we adopt a slightly large star formation efficiency, $\epsilon = 0.3$. Such a high star formation efficiency can be correct if a region is affected by the external pressure (Elmegreen & Efremov 1997).

In Fig. 7 (solid line), we show the evolution of gas temperature, ionisation degree, and molecular fraction for SBS 0335–052 with solid lines. The gas finally cools on a

timescale comparable to the observationally derived young age (~ 5 Myr): the temperature drops to $\lesssim 300$ K, the medium is kept neutral, and the molecular fraction increases. As mentioned in Section 2.2, the calculation is stopped at $t = t_{\text{gas}}/2$. However, since the gas state rapidly changes around $t = t_{\text{gas}}/2 = 5$ Myr, it is interesting to show the evolution after $t = t_{\text{gas}}/2$, although neglecting the gas consumption becomes a bad approximation. The dotted lines continuing after the solid lines show the evolutions for $t > t_{\text{gas}}/2$.

The evolutions of oxygen abundance and dust-to-gas ratio is also shown in Fig. 8 (solid line). The dashed lines shows the evolution after $t_{\text{gas}}/2$ (same as Fig. 7). We see that the metallicity reaches 1/50 solar (roughly the observational value 1/41 solar) around $t \sim 6$ Myr, which is marginally consistent with the age constraint by Vanzi et al. (2000) ($\lesssim 5$ Myr). We should note that this metallicity level is reached after $t_{\text{gas}}/2$, which implies that a significant fraction of gas in the star-forming region has been consumed. The run-away collapse of cooled gas could lead to such a rapid gas consumption. The dust-to-gas ratio is $\sim 10^{-4}$ at $t \sim 6$ Myr.

We have adopted a gas mass $M_{\text{gas}} \simeq 10^7 M_{\odot}$ for the star-forming region, much smaller than the observational estimate $\sim 10^9 M_{\odot}$ by Pustilnik et al. (2001) for the whole galaxy. However, because of the lack of resolution for H I observation, it is difficult to put a constraint on the gas mass in the star-forming region. There is also a large uncertainty in dust mass. Dale et al. (2001) estimate M_{dust} to be $2400 M_{\odot}$ but they neglect the stochastically heated dust grains (in this sense, the dust mass is underestimated), while Hunt et al. (2001) derive $10^5 M_{\odot}$, but they argue that this is an upper limit because of the assumed spatial filling factor of unity. From a radiative transfer model, which however neglects the effects of small grains, Plante & Sauvage (2002) find a dust mass of $1.5 \times 10^5 M_{\odot}$. Takeuchi et al. (2003) adopt the evolution model of HHF02, and they explain the infrared spectrum of SBS 0335–052 with $M_{\text{dust}} \sim 5 \times 10^3 M_{\odot}$, which is smaller than the upper limit by Hunt et al. (2001) but

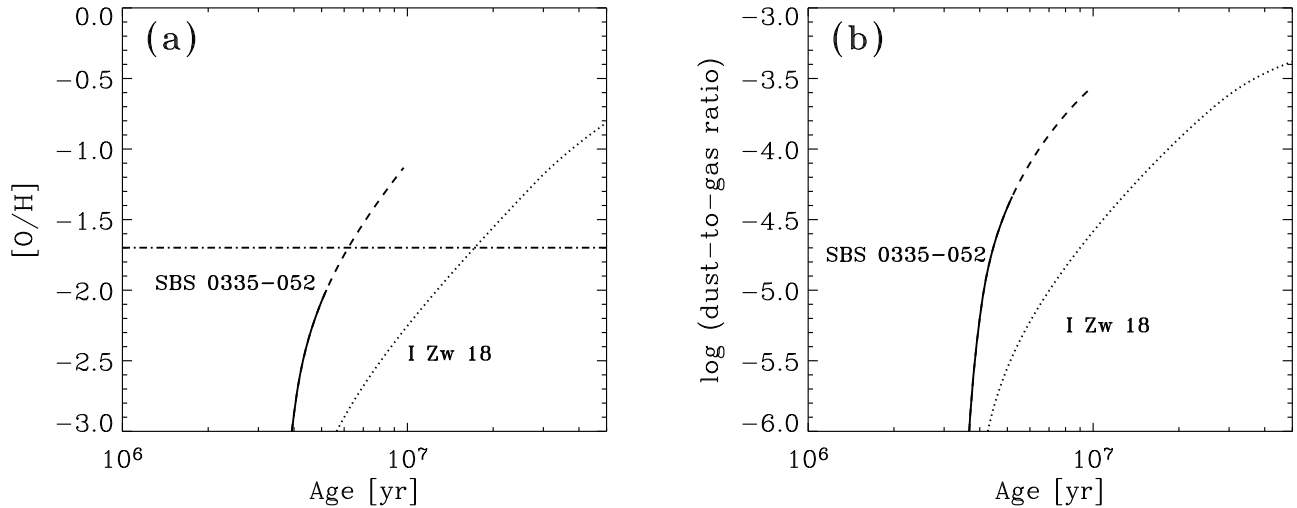


Fig. 8. Time evolution of **a)** metallicity and **b)** dust-to-gas ratio for the model of SBS 0335-052 and I Zw 18 (solid and dotted lines, respectively). The dashed line continuing from the solid line shows the evolution after t_{gas} . The dash-dotted line represents the metallicity level of 1/50 solar.

is larger than the possibly underestimated value by Dale et al. (2001).

By using $M_{\text{dust}} \sim 2 \times 10^3 - 10^5 M_{\odot}$ and $M_{\text{gas}} \sim 10^7 M_{\odot}$, we obtain a range of the dust-to-gas ratio in SBS 0335-052 of $2 \times 10^{-4} - 10^{-2}$, which is larger than that expected from our model. Because of the uncertainties in the dust mass and the gas mass, further observations are needed to better constrain these numbers for SBS 0335-052. Recently, Inoue (2003) also has discussed the dust-to-gas ratio of SBS 0335-052 with his model but he has reproduced the observational dust-to-gas ratio with $t \gtrsim 10^7$ yr. Nozawa et al. (2003) have proposed a SN dust production larger than Todini & Ferrara (2001), and their model could solve the discrepancy between theory and observation.

4.3. Possible intermediate active/passive BCDs

The active and passive modes of star formation are clearly two extremes on a continuum. In this paper, we have singled out two parameters that determine a galaxy’s position on this continuum, namely size r_{SF} and density n . Dust properties distinguish the two extremes, but they also must be viewed as part of a continuum of possibilities.

Figure 1 of HHTIV indicates that active and passive BCDs are clearly separated into two sequences in the surface brightness – density relation. However, there are BCDs which could be considered as intermediate between the active and passive extrema. For example, Mrk 71 (NGC 2366), whose metallicity is about 1/10 Z_{\odot} (Peimbert et al. 1986), has a compact star-forming region but a low surface brightness (Hunt et al., in preparation). Moreover, no SSCs are found in this galaxy by Billett et al. (2002). Another possible intermediate galaxy is Tol 1214-277, whose metallicity is about 1/25 Z_{\odot} (Izotov et al.

2001). It has a dense ($n \simeq 210 \text{ cm}^{-3}$; Fricke et al. 2001), but rather diffuse star-forming region (size ~ 200 pc; Hunt et al., in preparation). However, since this galaxy is distant (104 Mpc), it is difficult to constrain the size star-forming region of Tol 1214-277 even with the spatial resolution of *Hubble Space Telescope*.

5. Implications for high redshift

Large numbers of primeval galaxies are expected to exist in the high- z universe ($z \gtrsim 5$; e.g., Scannapieco et al. 2003). Because such galaxies must necessarily be chemically unevolved, it is useful to extend our concept of the active-passive dichotomy to high z . The “active” mode of star formation is particularly relevant for high- z galaxies, because of high gas density $\gtrsim 1000 \text{ cm}^{-3}$ (Norman & Spaans 1997) and warm dust content.

Galaxies become IR luminous on much shorter timescales than the cosmic age at $z \sim 5$ (HF02), even at metallicities is as low as I Zw 18 or SBS 0335-052 (see also Morgan & Edmunds 2003). We have shown that during an “active” star formation episode with no prior chemical enrichment, dust produced by SNe II efficiently shields the UV radiation. This means that the heating by UV photons in the ISM is not sufficient to halt gas cooling. Therefore, it is important to trace the high- z star formation activity in the IR (or sub-mm) (e.g., Chapman et al. 2001). Indeed, large extinction has been shown by some samples of high- z galaxies (e.g., Meurer et al. 1999; Stanway et al. 2003).

The “active” mode is also characterised by high dust temperature ($\gtrsim 40$ K) because of the high UV interstellar radiation field. Totani & Takeuchi (2002) have shown that the existence of high temperature dust at $z \sim 3$ is favoured to explain the far-IR cosmic background radiation. Thus,

it is important to investigate a potential increase of the “active” star formation mode at high z (especially the increase of a population with high dust temperature), in order to quantify the contribution of such galaxies to the cosmic IR background.

Indeed, virtually all high-redshift star formation may occur in the “active” regime. It is not clear whether there are high z objects corresponding to the “passive” mode of star formation. H_2 has been difficult to detect from damped Ly α clouds (DLAs; e.g., Petitjean et al. 2002; Ledoux et al. 2003). In general, stringent upper limits of $\lesssim 10^{-6}$ have been placed on the molecular fractions for DLAs. In passive star-forming regions, the molecular fraction is kept as low as $\sim 10^{-5}$ on timescales of several tens of Myr. Therefore, some of the DLAs could be “passive” star-forming objects. However, the low abundance of molecules can also be explained by photodissociation by the cosmic UV background radiation (e.g., Hirashita et al. 2003).

6. Conclusions

In this paper, we have theoretically modeled the “active” and “passive” star formation modes observed in metal-poor BCDs. The “active” mode is characterised by dense and compact ($n \gtrsim 500 \text{ cm}^{-3}$ and $r_{\text{SF}} \lesssim 50 \text{ pc}$) star-forming regions. On the contrary, the “passive” mode takes place in diffuse ($n \lesssim 100 \text{ cm}^{-3}$ and $r_{\text{SF}} \gtrsim 100 \text{ pc}$) star-forming regions.

In the dense regions observed in “active” BCDs, the gas free-fall time is typically shorter than $\sim 5 \text{ Myr}$. Such a short free-fall time can enhance star formation activity and generate an efficient supply of dust from SNe II. An accumulation of dust in such a compact region leads to a large dust optical depth, and the region consequently becomes luminous in the IR. Even in the environment of active star formation, the gas retains the physical conditions favourable for the gas collapse: cool ($\lesssim 1000 \text{ K}$) and highly molecular ($f_{\text{H}_2} \gtrsim 10^{-2}$). The above characteristics explain the properties of star-forming regions in the BCDs categorised as “active” in HHTIV, especially SBS 0335–052 (i.e., IR luminous, containing hot dust, rich in molecules, compact, and dense).

In “passive” BCDs, the dynamical time of diffuse regions is longer than 10^7 yr , and the star formation rate can be as low as $\lesssim 0.1 M_{\odot}$. The increase of dust optical depth is milder and therefore “passive” star-forming regions become IR luminous much later in their evolution, $> 10^7 \text{ yr}$. Such a passive region has a low $\lesssim 10^{-4}$ molecular content, and it would be difficult to detect H_2 in passive BCDs.

However, the physical state of gas is strongly affected by the size and spatial distribution of grains. With a fixed total dust mass, if the grain radius is large, the optical depth of dust against the UV light is small. This means for large grains ($\sim 0.01 \mu\text{m}$), the gas temperature and ionisation degree tend to be high, and the molecular fraction tends to be low. As for the spatial distribution of grains, efficient shielding of UV light takes place in a screen ge-

ometry, which leads to efficient cooling and molecule formation. On the contrary, in the mixed geometry, because of inefficient shielding, the gas is heated to nearly 10^4 K , and the molecules are efficiently dissociated.

We also discussed the evolution of dust-to-gas ratio and metallicity. In particular, our model is consistent with the observations of I Zw 18 and SBS 0335–052, but future observations of dust in metal-poor ($[\text{O}/\text{H}] \lesssim -1$) BCDs are needed for further constraints. The consistency also implies that around 10–20 % of metals supplied from SNe are in the dust phase.

We have shown how differences in two physical parameters of a star-forming region, its size and density, can lead to substantially different evolution over time. The distinction has been made between “active” and “passive” modes, but such a dichotomy is perhaps misleading, since they are rather extremes on a continuum. Pressure must also drive evolution of a star-forming region, and may determine a region’s initial size and density. However, after the onset of star formation, dust shielding of UV photons determines the fate of star-forming regions, which finally bifurcates into active and passive regimes.

Acknowledgements. We thank the anonymous referee for useful comments which improved this paper considerably. We are grateful to T. X. Thuan, A. Ferrara, M. A. R. Kobayashi, and H. Shibai for stimulating discussions on galaxy evolution. H. H. was supported by the Research Fellowship of the Japan Society for the Promotion of Science for Young Scientists. We fully utilised the NASA’s Astrophysics Data System Abstract Service (ADS).

Appendix A: Equilibrium dust temperature

We derive and discuss the equilibrium dust temperature in Eq. (21). We start from the following equation between absorbed and emitted energy of a grain:

$$cu_{\text{UV}}\pi a^2 Q_{\text{UV}} = 4\pi a^2 \int_0^{\infty} Q_{\text{IR}}(a, \lambda) \pi B_{\lambda}(T_{\text{dust}}) d\lambda, \quad (\text{A.1})$$

where u_{UV} is the radiative energy in UV defined in Eq. (2), a is the grain radius, $B_{\lambda}(T_{\text{dust}})$ is the Planck function estimated at the wavelength of λ and the dust temperature of T_{dust} , and Q_{UV} and $Q_{\text{IR}}(a, \lambda)$ are the absorption cross sections of a grain normalized by the geometrical cross section in UV and IR, respectively. We assume that Q_{UV} is independent of λ (Draine & Lee 1984), and adopt the following form for $Q_{\text{IR}}(a, \lambda)$:

$$Q_{\text{IR}}(a, \lambda) = \frac{2\pi Aa}{\lambda^{\beta}}, \quad (\text{A.2})$$

In the main text, we assume that $\beta = 2$ (Drapatz & Michel 1977; Shibai et al. 1999; Takeuchi et al. 2003), but we generalise the wavelength dependence. Since the Planck function is written as

$$B_{\lambda}(T) = \frac{2hc^2/\lambda^5}{\exp(hc/\lambda kT) - 1}, \quad (\text{A.3})$$

where k is the Boltzmann constant, we obtain the following analytic solution for T_{dust} :

$$T_{\text{dust}} = \frac{hc}{k} \left(\frac{u_{\text{UV}} Q_{\text{UV}}}{16\pi^2 A a h c I(3 + \beta)} \right)^{1/(4+\beta)}, \quad (\text{A.4})$$

where the function $I(\alpha)$ is defined as

$$I(\alpha) \equiv \int_0^\infty \frac{x^\alpha}{e^x - 1} dx \quad (\alpha > 0). \quad (\text{A.5})$$

Since $I(5) = 8\pi^6/63$, we obtain Eq. (21) for $\beta = 2$.

References

- Abel, T., Bryan, G. L., & Norman, M. L. 2000, *ApJ*, 540, 39
- Aloisi, A., Tosi, M., & Greggio, L. 1999, *AJ*, 118, 302
- Alton, P. B., Lequeux, J., Bianchi, S., et al. 2001, *A&A*, 366, 451
- Barkana, R. 2002, *NewA*, 7, 85
- Bekki, K., & Couch, W. J. 2001, *ApJ*, 557, L19
- Bendo, G. J., Joseph, R. D., Wells, M., et al. 2002, *AJ*, 124, 1380
- Bianchi, S., Davies, J. I., & Alton, P. B. 1999, *A&A*, 344, L1
- Billett, O. H., Hunter, D. A., & Elmegreen, B. G. 2002, *AJ*, 123, 1454
- Bonnor, W. B. 1956, *MNRAS*, 116, 351
- Boulanger, F., Beichman, C., Désert, F. X., Helou, G., Péroul, M., & Ryter, C. 1988, *ApJ*, 332, 328
- Bromm, V., Coppi, P. S., & Larson, R. B. 2001, *ApJ*, 564, 23
- Cannon, J. M., Skillman, E. D., Garnett, D. R., & Dufour, R. J. 2002, *ApJ*, 565, 931
- Cazaux, S., & Tielens, A. G. G. M. 2002, *ApJ*, 575, L29
- Chapman, S. C., Richards, E. A., Lewis, G. F., Wilson, G., & Barger, A. J. 2001, *ApJ*, 548, 147
- Ciardi, B., Ferrara, A., Governato, F., & Jenkins, A. 2000, *MNRAS*, 314, 611
- Contursi, A., Lequeux, J., Cesarsky, D., et al. 2000, *A&A*, 362, 310
- Cox, A. N. 2000, *Allen's Astrophysical Quantities*, 4th ed. (Springer, New York)
- Dale, D. A., Helou, G., Neugebauer, G., Soifer, B. T., Frayer, D. T., & Condon, J. J. 2001, *AJ*, 122, 1736
- Draine, B. T., & Lee, H. M. 1984, *ApJ*, 285, 89
- Drapatz, S., & Michel, K. W. 1977, *A&A*, 56, 353
- Dwek, E., & Scalo, J. M. 1980, *ApJ*, 239, 193
- Dwek, E. 1998, *ApJ*, 501, 643
- Ebert, R. 1955, *Z. Astrophys.*, 37, 222
- Elmegreen, B. G. 2000, *ApJ*, 530, 277
- Elmegreen, B. G., & Efremov, Y. N. 1997, *ApJ*, 480, 235
- Elmegreen, B. G., & Elmegreen, D. M. 1978, *ApJ*, 220, 1051
- Elmegreen, B. G., & Hunter, D. A. 2000, *ApJ*, 540, 814
- Peimbert, M., Peña, M., & Torres-Peimbert, S. 1986, *A&A*, 158, 266
- Ferrara, A., Pettini, M., & Shchekinov, Y. 2000, *MNRAS*, 319, 539
- Fricke, K. J., Izotov, Y. I., Papaderos, P., et al. 2001, *AJ*, 121, 169
- Galli, D., & Palla, F. 1998, *A&A*, 335, 403
- Galliano, F., Madden, S. C., Jones, A. P., et al. 2003, *A&A*, 407, 159
- Habart, E., Boulanger, F., Verstraete, L., et al. 2003, *A&A*, 397, 623
- Hildebrand, R. H. 1983, *QJRAS*, 24, 267
- Hirashita, H., & Ferrara, A. 2002, *MNRAS*, 337, 921 (HF02)
- Hirashita, H., Ferrara, A., Wada, K., & Richter, P. 2003, *MNRAS*, 341, L18
- Hirashita, H., Hunt, L. K., & Ferrara, A. 2002, *MNRAS*, 330, L19 (HHF02)
- Hopkins, A. M., Schulte-Ladbeck, R. E., Drozdovsky, I. O. 2002, *AJ*, 124, 862
- Hunt, L. K., Giovanardi, C., & Helou, G. 2002, *A&A*, 394, 873
- Hunt, L.K., Dyer, K.D., Thuan, T.X., Ulvestad, J.S. 2004a, *ApJ*, submitted
- Hunt, L. K., Hirashita, H., & Thuan, T. X. 2004b, in preparation
- Hunt, L.K., Hirashita, H., Thuan, T.X., Izotov, Y.I., & Vanzi, L. 2003a, in Proceedings of "Galaxy Evolution: Theory and Observations", Eds. V. Avila-Reese, C. Firmani, C. Frenk, & C. Allen, *RevMexAA SC (HHTIV) (astro-ph/0310865)*
- Hunt, L. K., Thuan, T. X., & Izotov, Y. I. 2003b, *ApJ*, 588, 281
- Hunt, L. K., Vanzi, L., & Thuan, T. X. 2001, *A&A*, 377, 66
- Hunter, D. A., O'Connell, R. W., & Gallagher, J. S. III, 1994, *AJ*, 108, 84
- Inoue, A. K. 2003, *PASJ*, 55, 901
- Inoue, A. K., Hirashita, H., & Kamaya, H. 2000, *AJ*, 120, 2415
- Inoue, A. K., Hirashita, H., & Kamaya, H. 2000, *ApJ*, 555, 613
- Izotov, Y. I., Chaffee, F. H., Foltz, C. B., et al. 1999, *ApJ*, 527, 757
- Izotov, Y. I., Chaffee, F. H., & Green, R. F. 2001, *ApJ*, 562, 727
- Izotov, Y. I., & Thuan, T. X. 1999, *ApJ*, 511, 639
- James, A., Dunne, L., Eales, S., & Edmunds, M. G. 2002, *MNRAS*, 335, 753
- Jones, A. P., Tielens, A. G. G. M., & Hollenbach, D. J. 1996, *ApJ*, 469, 740
- Kamaya, H., & Hirashita, H. 2001, *PASJ*, 53, 483
- Kamaya, H., & Silk, J. 2002, *MNRAS*, 332, 251
- Kitayama, T., & Ikeuchi, S. 2000, *ApJ*, 529, 615
- Kitayama, T., Susa, H., Umemura, M., & Ikeuchi, S. 2001, *MNRAS*, 326, 1353
- Kozasa, T., Hasegawa, H., & Nomoto, K. 1989, *ApJ*, 344, 325
- Kunth, D., & Östlin, G. 2000, *A&AR*, 10, 1
- Ledoux, C., Petitjean, P., & Srianand, R. 2003, *MNRAS*, 346, 209
- Lin, D. N. C., & Murray, S. D. 1992, *ApJ*, 394, 523
- Lisenfeld, U., & Ferrara, A. 1998, *ApJ*, 496, 145
- Matsuda, T., Sato, H., & Takeda, H. 1968, *Prog. Theor. Phys.*, 42, 219
- Meurer, G. R., Heckman, T. M., & Calzetti, D. 1999, *ApJ*, 521, 64
- McKee, C. F. 1989, in *IAU Symp. 135, Interstellar Dust*, ed. L. J. Allamandola & A. G. G. M. Tielens (Dordrecht: Kluwer), 431
- Morgan, H. L., & Edmunds, M. G. 2003, *MNRAS*, 343, 427
- Natta, A., & Panagia, N. 1984, *ApJ*, 287, 228
- Nishi, R., Susa, H., Uehara, H., et al. 1998, *Prog. Theor. Phys.*, 100, 881
- Norman, C. A., & Spaans, M. 1997, *ApJ*, 480, 145
- Nozawa, T., Kozasa, T., Umeda, H., et al. 2003, *ApJ*, 598, 785
- Omukai, K. 2000, *ApJ*, 534, 809
- Östlin, G. 2000, *ApJ*, 535, L99
- Peebles, P. J. E., & Dicke, R. H. 1968, *ApJ*, 154, 891
- Petitjean, P., Srianand, R., & Ledoux, C. 2002, *MNRAS*, 332, 383

- Plante, S., & Sauvage, M. 2002, *AJ*, 124, 1995
- Popescu, C. C., Hopp, U., & Rosa, M. R. 1999, *A&A*, 350, 414
- Puget, J. L., & Léger, A. 1989, *ARA&A*, 27, 161
- Pustilnik, S. A., Brinks, E., Thuan, T. X., Lipovetsky, V. A., & Izotov, Y. I. 2001, *AJ*, 121, 1413
- Recchi, S., Matteucci, F., D'Erdole, A., & Tosi, M. 2002, *A&A*, 384, 799
- Ripamonti, E., Haardt, F., Ferrara, A., & Colpi, M. 2002, *MNRAS*, 334, 401
- Salvaterra, R., & Ferrara, A. 2003, *MNRAS*, 339, 973
- Scannapieco, E., Schneider, R., & Ferrara, A. 2003, *ApJ*, 589, 35
- Schaerer, D. 2002, *A&A*, 382, 28
- Schneider, R., Ferrara, A., & Salvaterra, R. 2004, *MNRAS*, submitted
- Searle, L., & Sargent, W. L. W. 1972, *ApJ*, 173, 25
- Shibai, H., Okumura, K., & Onaka, T. 1999, *Star Formation 1999*, ed. T. Nakamoto (Nobeyama: Nobeyama Radio Observatory), 67
- Silva, L., Granato, G. L., Bressan, A., & Danese, L. 1998, *ApJ*, 509, 103
- Skillman, E. D., & Kennicutt, R. C., Jr. 1993, *ApJ*, 411, 655
- Smail, I., Ivison, R. J., & Blain, A. W. 1997, *ApJ*, 490, L5
- Stanway, E. R., Bunker, A. J., & McMahon, R. G. 2003, *MNRAS*, 342, 439
- Takeuchi, T. T., Hirashita, H., Ishii, T. T., Hunt, L. K., & Ferrara, A. 2003, *MNRAS*, 343, 839
- Takeuchi, T. T., Yoshikawa, K., & Tomita, A. 2004, *ApJ*, submitted
- Tegmark, M., Silk, J., Rees, M. J., et al. 1997, *ApJ*, 474, 1
- Thuan, T. X., Sauvage, M., & Madden, S. 1999, *ApJ*, 516, 783
- Tielens, A. G. G. M. 1998, *ApJ*, 499, 267
- Tinsley, B. M. 1980, *Fundam. Cosmic Phys.*, 5, 287
- Todini, P., & Ferrara, A. 2001, *MNRAS*, 325, 726
- Tomita, A., Yoshikawa, K., Takeuchi, T. T., Hirashita, H. 2002, in *Proc. of the IAU 8th Asian-Pacific Regional Meeting, Vol. II*, ed. S. Ikeuchi, J. Hearnshaw, T. Hanawa, (Tokyo: Astronomical Society of Japan), 301
- Totani, T., & Takeuchi, T. T. 2002, *ApJ*, 570, 470
- Tsujimoto, T., Yoshii, Y., Nomoto, K., et al. 1997, *ApJ*, 483, 228
- van Zee, L., Westpfahl, D., Haynes, M. P., & Salzer, J. J. 1998, *AJ*, 115, 1000
- Vanzi, L., Hunt, L. K., Thuan, T. X., & Izotov, Y. I. 2000, *A&A*, 363, 493
- Vidal-Madjar, A., Kunth, D., Lecavelier des Etangs, A., et al. 2000, *ApJ*, 538, L77
- Voit, G.M. 1992, *MNRAS*, 258, 841
- Walter, F., Weiss, A., Martin, C., & Scoville, N. 2002, *AJ*, 123, 225
- Wilson, C. D., Scoville, N., Madden, S. C., & Charmandaris, V. 2000, *ApJ*, 542, 120
- Woosley, S. E., & Weaver, T. A. 1995, *ApJS*, 101, 181